Experimental contribution to the corium thermodynamic modelling – The U–Zr–Al–Ca–Si–O system

Andrea Quaini, Christine Guéneau, Stéphane Gossé, Thierry Alpettaz, Emmanuelle Brackx, Renaud Domenger, Anne Chocard, Fiqiri Hodaj

Experimental contribution to the corium thermodynamic modelling – The U–Zr–Al–Ca–Si–O system

A. Quaini [a,*], C. Guéneau [a], S. Gossé [a], T. Alpettaz [a], E. Brackx [b], R. Domenger [b], A. Chocard [b], F. Hodaj [c,d]

[a] CEA, DPC, SCCME, LM2T, Centre de Saclay, 91191 Gif-sur-Yvette Cedex, France
[b] CEA Marcoule, DEN, DTEC, SGCS, LMAC, 30207 Bagnols-sur-Cèze, France
[c] Univ. Grenoble Alpes, SIMAP, F-38000 Grenoble, France
[d] CNRS, Grenoble INP, SIMAP, F-38000 Grenoble, France

During a severe accident in a nuclear reactor, extreme temperatures may be reached (T > 2500 K). In these conditions, the nuclear fuel may react with the Zircaloy cladding and then with the steel vessel, forming a mixture of solid–liquid phases called in-vessel corium. In the worst scenario, this mixture may penetrate the vessel and reach the concrete underneath the reactor. In order to develop the TAF-ID thermodynamic database (www.oecd-nea.org/science/taf-id) on nuclear fuels and to predict the high temperature beha-viour of the corium + concrete system, new high temperature thermodynamic data are needed. The LM2T at CEA Saclay centre started an experimental campaign of phase equilibria measurements at high temper-ature (up to 2600 K) on interesting corium sub-systems. In particular, a heat treatment at 2500 K has been performed on two prototypic ex-vessel corium samples (within the U–Zr–Al–Ca–Si–O system) with different amounts of CaO and SiO_2. The results show that depending on the SiO_2-content, the final con-figuration of the samples can be significantly different. The sample with the higher CaO-content showed a dendritic structure representative of a single quenched liquid phase, whilst the sample richer in SiO_2 exhibited a microstructure which suggests the presence of a liquid miscibility gap. Furthermore a new laser heating setup has been conceived. This technique allows very high temperature measures (T > 3000 K) limiting the interactions between the sample and the surroundings.

1. Introduction

During a severe accident in a nuclear power reactor, a mixture of solid and liquid phase called corium may form inside the reactor vessel due to the chemical interaction between the fuel UO_2, the Zircaloy cladding and the steel vessel. The high temperature behaviour of the chemical system U–Zr–Fe–O strongly affects the accidental scenario proceedings. In the case of loss of the mechanical strength of the reactor steel vessel, the molten corium may reach the concrete (Al_2O_3–CaO–SiO_2) in the cavity underneath the vessel: in this scenario the more complex U–Zr–Fe–Ca–Si–Al–O system is concerned. Many phenomena take place during Molten Corium Concrete Interaction MCCI (Journeau and Piluso, 2012): high temperature concrete decomposition, heat transfer due to gas bubbles agitation, formation of several phases, oxidation of metals, etc. Several studies on the interaction between corium and concrete were published starting from the 1980s; in particular, numerous large-scale experiments were performed on this subject. Journeau and Piluso (2012) reported an exhaustive list of the early MCCI experiments as well as more recent MCCI projects. All these studies gave valuable data for a better comprehension of the phenomena occurring after the interaction between molten corium and concrete. However extensive uncertainties still exist on various aspects of MCCI scenarios. The complexity of the concerned chemical system, the extreme temperature and pressure conditions and the elevated number of possible accidental scenarios make the MCCI studies rather intricate.

Although large-scale experiments give information on macroscale phenomena, such as ablation profile, corium flooding behaviour, coolability of the molten core, density and viscosity evolution, the interpretation of the sample microstructure is challenging. In fact, the large dimensions of the samples cause temperature and composition gradients between the centre and the periphery of the sample as shown for example by Journeau et al. (2001).

In this framework a campaign of small-scale experiments is ongoing at the Laboratoire de Modélisation, de Thermodynamique

* Corresponding author. Tel.: +33 (0)1 69 08 21 70.
E-mail address: andrea.quaini@cea.fr (A. Quaini).

et de Thermochimie (LM2T), CEA Saclay. At the moment, two series of experiments were performed:

- The first series was dedicated to the study of the liquid immiscibility in the U–Zr–O ternary system. The liquid miscibility gap has been studied in the past (Juenke and White, 1970; Guéneau et al., 1998). However, some experimental and modelling discrepancies still exist, in particular on the extension of the immiscibility region (Guéneau et al., 1998; Chevalier et al., 2004). Novel experimental results allowed to obtain two tie-lines in the ternary miscibility gap. Details on this series of experiments will be soon published in a separate paper (Quaini et al., submitted for publication).
- The second series of small-scale experiments was devoted to the investigation of the corium/concrete interaction. In particular, two samples have been investigated for a better comprehension of the interaction between a simplified corium and concrete. The experimental details and the results on this study are reported in the present paper.

In parallel the development of TAF-ID thermodynamic database is ongoing. This database is developed in the framework of an OECD–NEA project (Organisation for Economic Co-operation and Development–Nuclear Energy Agency). Several groups of research gather their calculation tools and thermodynamic database into the TAF-ID project. At the present stage Canada, France, Japan, The Netherlands, Republic of Korea and USA actively contribute to the development of the TAF-ID database. The main objective of the TAF-ID project is to assure a comprehensive and reliable international thermodynamic database for the calculation of phase diagram and thermodynamic properties of advanced nuclear fuel, fission products and structural materials (steel, Zircaloy, concrete). The TAF-ID database can be coupled with severe accident codes to predict the high temperature behaviour of the corium + concrete system during an accidental scenario.

Finally, the innovative high temperature setup called ATTILHA, conceived and developed at the LM2T will be presented. This experimental facility will allow precise measurement in a wide temperature range (1500–3000 K). The coupling of a laser heating technique with an aerodynamic levitation setup will allow investigating systems whereof contactless conditions are paramount.

2. Materials and methods

During the present work, heat treatments were performed in a Joule effect furnace (W-resistor) represented schematically in Fig. 1. This furnace is usually employed for high temperature mass spectrometer measurement (Baichi et al., 2001). The annealing tests are performed under very high vacuum ($p \sim 10^{-7}$ Pa). The temperature is monitored by using a calibrated IMPAC ISR-900 two-channel optical pyrometer.

Two samples within the U–Zr–Al–Ca–Si–O system were investigated. These samples are constituted by UO_2–ZrO_2–Al_2O_3–CaO–SiO_2 to simulate the interaction between a simplified corium (UO_2–ZrO_2) and concrete (Al_2O_3–CaO–SiO_2). During the present work, Fe was not considered.

The initial compositions of the samples were calculated by A. Boulin (LPMA, CEA Cadarache) with TOLBIAC-ICB software (Spindler et al., 2006). The calculation was performed assuming an oxidised corium only composed by UO_2 (80 tons) and ZrO_2 (20 tons). The whole mass of molten corium at 2950 K pours onto the concrete slab. Two types of concrete were considered: a limestone concrete (rich in CaO) and a siliceous concrete (rich in SiO_2). The composition of the samples corresponds to that of the liquid pools (CORIUM_1 for the interaction with limestone concrete, CORIUM_2 for the interaction with siliceous concrete) 24 h after the corium/concrete interaction (CCI). The aim is to study the effect of the concrete composition (i.e., the SiO_2 content) on the final configuration of the samples.

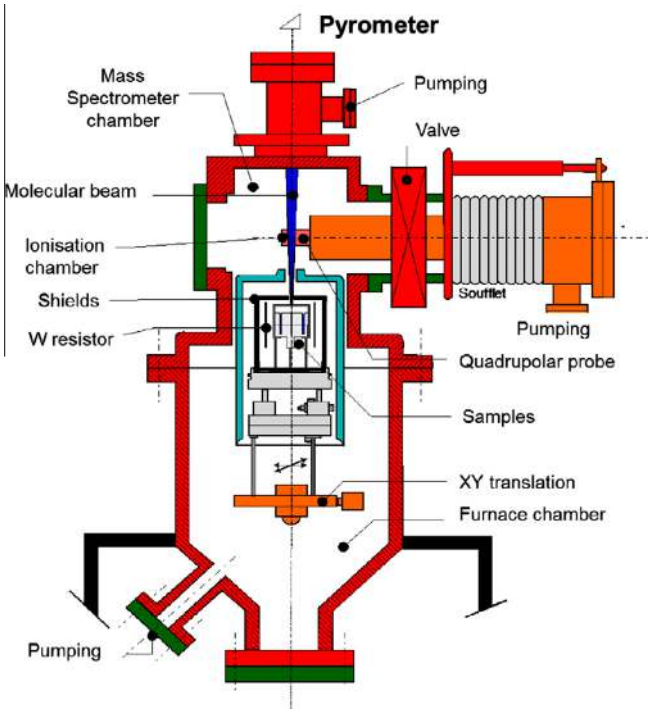

Fig. 1. Schematic view of the furnace employed for the annealing tests.

The samples were directly fabricated by mixing the starting materials in W-crucible (with screwed lid). The starting materials were Al_2O_3 powder (Alfa Aesar, 99.997%), CaO powder (SCM, 99.9%), SiO_2 spheres (SCM, 99.995%), UO_2 powder (CEA supply, 99.996%) and ZrO_2 powder (Goodfellow, purity 99.9%). The compositions of the samples are reported in Table 1.

The samples underwent a heat treatment for 30 min at 2500 ± 25 K and then they were cooled (3 K/s). The samples were then analysed at the LMAC, CEA Marcoule. For the characterisation a Carl Zeiss Merlin scanning electron microscope equipped with a Field Emission Gun (SEM-FEG) was used. It is coupled with energy dispersion spectroscopy (EDS, Oxford Instruments X-MAX 80 mm^2) and a wavelength-dispersive X-ray spectroscope (WDS, SX 100 CAMECA). The standards used for the analyses were UO_2 for uranium, $CaSiO_3$ for calcium and oxygen, SiO_2 for silicon, Zr for zirconium, W for tungsten and Al for aluminium.

3. Results and discussion

In the following, the experimental results obtained on the two investigated samples are reported. The differences observed in the samples will be discussed.

Table 1
Compositions of the in vessel corium + concrete samples (in mass percentage).

	CORIUM_1	CORIUM_2
Al_2O_3	1.8	2.1
CaO	32.4	11.0
SiO_2	24.6	64.0
UO_2	30.8	15.4
ZrO_2	10.4	7.8

3.1. Sample CORIUM_1

Fig. 2a shows a backscattering electrons (BSE) image of the microstructure of sample CORIUM_1 after the cooling.

The solidified sample has a homogenous dendritic structure, suggesting that a single liquid phase was present at 2500 K (Fig. 2b). EDS and WDS analyses revealed a negligible amount of W (coming from the W crucible) dissolved in the sample (less than 0.5 at.%). The measured compositions of the identified phases are reported in Table 2.

The white dendrites in Fig. 2c were identified as a face centred cubic (fcc) $(U,Zr,Ca)O_2$ phase. Precipitates of the same type of phase $(Zr,U,Ca)O_2$ are located around. The difference between those phases is the U content. While in the lighter one (white dendrites) the main metallic element is U, the other is richer in Zr. Ca is the minor metallic element in both phases. The dark matrix is basically oxide, and it is enriched in Ca and Si with small amounts of Al and Zr. This zone was indexed as a Rankinite-like phase $(Ca,Al,Zr)_3Si_2O_7$. It can be also noted a fourth minor phase. This phase contains a significant amount of Zr and a small quantity of U. The major metallic elements are Ca and Si. The phase $(Ca,Zr,U)_2SiO_4$ can fit the current EDS and WDS results. The EDS results on sample CORIUM_1 are reported in Table 2.

3.2. Sample CORIUM_2

In Fig. 3 the microstructure of sample CORIUM_2 is reported. The observed microstructure is radically different compared to what is observed in sample CORIUM_1. In fact, the microstructure is extremely fine. On the top right side of the sample cross section, a region with a different chemical contrast may be noted (Zone 2 in Fig. 3a). Fig. 3b shows a third region between Zone 1 and Zone 2. This region named "Transition zone" is about 50–100 μm thick and its microstructure is a combination of those of Zone 1 and Zone 2. The BSE image in Fig. 3c reports the microstructure of Zone 1. Black droplets of about 1–3 μm in diameter are dispersed within a complex structure composed of a white region and a grey phase. The white region is heterogeneous and it seems to be constituted of several phases, which, however, are too small to be characterised.

EDS analyses on this zone of the sample (Table 3) revealed that the black region is basically SiO_2, since the amount of the other metallic elements (i.e., Al, Ca, U and Zr) are under the limit of detection of the current spectrometer. The white region and the grey phase are rich in Si. The main difference is that the white phase has a significant amount of U. The amount of U measured in the grey phase is under the limit of detection of the spectrometer.

Zone 1 is separated from the Transition zone by an interface (Fig. 3b). Transition zone is formed by a black matrix with a fine dispersion of white droplets (Fig. 3d). White structures formed by several phases and similar to those observed in Zone 1 can be also noted. A second interface separates the Transition zone and Zone 2 (Fig. 3d and e). The latter is formed by a very fine dispersion of white droplets (Fig 3e) within a black matrix. The droplets have the same overall composition of the white structures observed in Zone 1 and Transition zone. The black matrix seems to be very similar to that observed in Zone 1. However a direct analysis of Zone 2 was not possible. In fact, this region is proved to be fragile once confronted to the SEM electron beam, which causes a hole on the surface of the polished surface of the sample making quantitative analyses impossible. This is possibly due to the amorphous nature of the concerned zone of the sample.

The complex structure of the white droplets/structures observed in sample CORIUM_2 can be seen in Fig. 3e. Dendrites of a white phase are surrounded by an amorphous light grey phase. These phases have the same structures of those observed in Zone 1.

The drop-shaped structures observed in Fig. 3 are characteristic of the presence of two immiscible liquids, one enriched in U (i.e., the white structure) and the other richer in SiO_2 (i.e., the black structures). It can be noted that in Zone 1 black droplets are dispersed within a white structure, forming a sort of porous network. In Zone

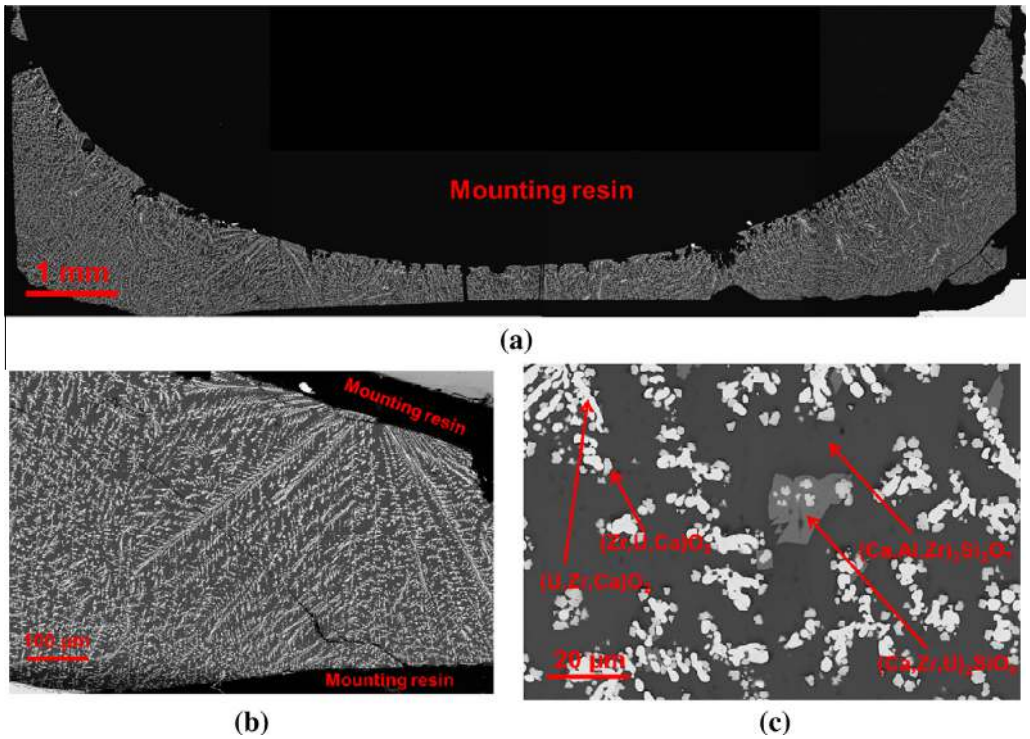

Fig. 2. BSE images of sample CORIUM_1. (a) Cross section; (b) magnification on the solidified sample; (c) identified phases within the solidified sample.

Table 2
EDS results on sample CORIUM_1 (the results are reported in atomic percent).

	Al	Ca	Si	U	Zr	O	
Initial	1.2	18.8	13.3	3.7	2.8	60.2	
Overall	1.5 ± 1.0	18.0 ± 2.0	16.0 ± 2.0	2.5 ± 0.5	2.0 ± 0.2	60.0 ± 5.0	
Dendrites 1	/	3.0 ± 0.5	/	22.0 ± 1.0	7.0 ± 1.0	68.0 ± 2.0	$(U,Zr,Ca)O_2$
Dendrites 2	/	5.0 ± 1.0	/	11.5 ± 2.0	16.6 ± 2.0	67.4 ± 3.0	$(Zr,U,Ca)O_2$
Minor grey phase	/	21.0 ± 2.0	13.5 ± 2.0	1.0 ± 1.0	5.0 ± 1.0	59.5 ± 2.0	$(Ca,Zr,U)_2SiO_4$
Dark matrix	1.5 ± 1.0	20.5 ± 2.0	17.0 ± 2.0	/	1.0 ± 1.0	60.0 ± 2.0	$(Ca,Al,Zr)_3Si_2O_7$

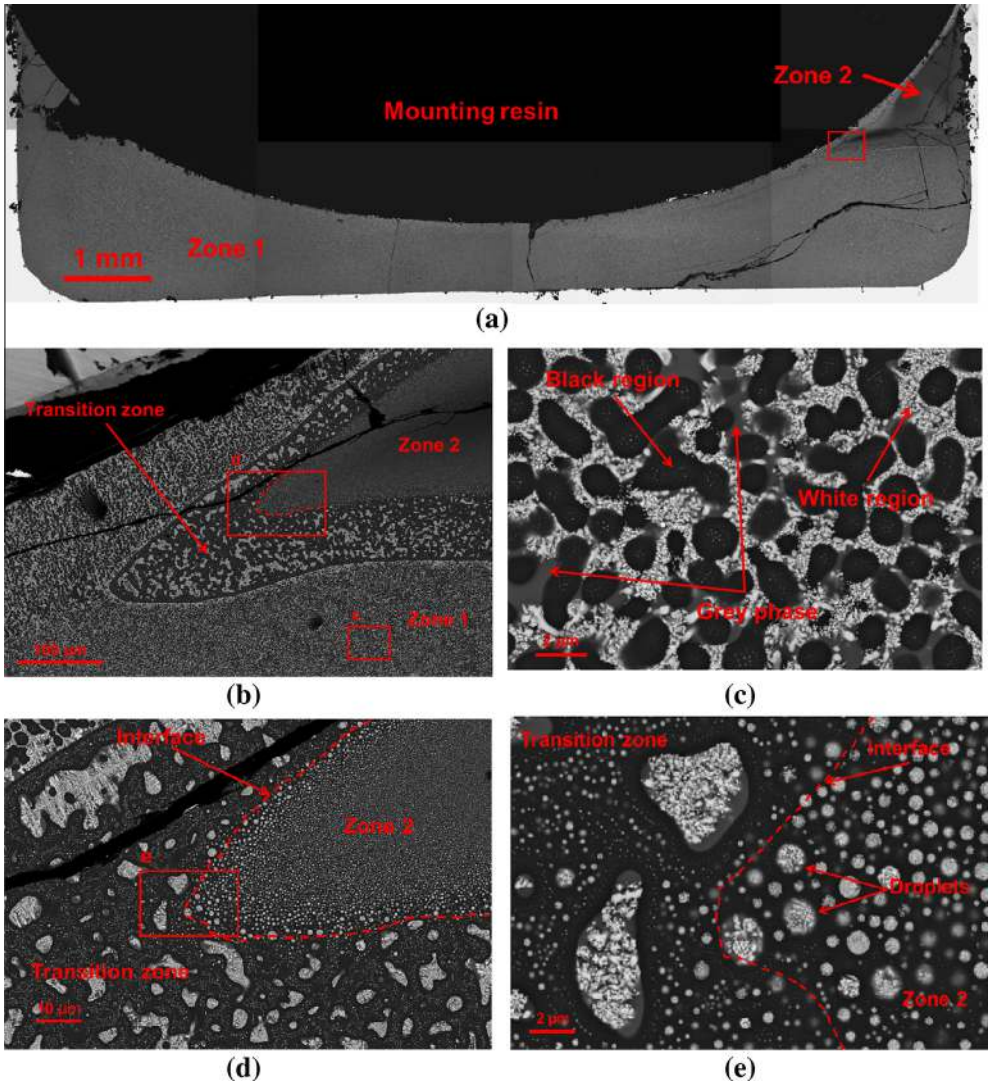

Fig. 3. BSE images of sample CORIUM_2. (a) Cross section of the solidified sample; (b) close-up view of the interface between Zone 1 and Zone 2. The major regions are separated by a third region named "Transition zone"; (c) magnification on Zone 1; (d) magnification on the interface between Transition zone and Zone 2; (e) close-up on the interface Transition zone/Zone 2.

Table 3
EDS analyses on Zone 1.

	at.% Al	at.% Ca	at.% Si	at.% U	at.% Zr	at.% O
Overall	0.9 ± 0.5	3.9 ± 1.0	25.9 ± 2.0	1.3 ± 1.0	1.7 ± 1.0	66.3 ± 3.0
White region	1.3 ± 1.0	4.4 ± 1.0	20.8 ± 2.0	4.3 ± 1.0	3.7 ± 1.0	65.5 ± 3.0
Black region	0.4 ± 0.4	0.8 ± 0.8	31.5 ± 3.0	0.2 ± 0.4	0.4 ± 0.4	66.7 ± 3.0
Grey phase	2.2 ± 1.0	7.7 ± 1.0	24.6 ± 2.0	0.2 ± 0.2	1.1 ± 1.0	64.2 ± 3.0

2 white droplets are dispersed within a black structure. In both zones, the droplets are homogenously dispersed. The Transition zone plays the role of interface between the Zone 1 and Zone 2.

Gusarov et al. (2006) studied the extension of the miscibility gap in the UO_2–SiO_2 system. The authors showed that above 2273 K a separation in two layers occurs. SEM-EDS analyses revealed that the upper layer was enriched in SiO_2, whilst the bottom one was enriched in UO_2. A boundary region, comparable to the current Transition zone, was also observed. The observed microstructures are very similar to those observed during the present investigation. The UO_2-rich layer was characterised by a fine dispersion of black droplets (basically SiO_2) within a white matrix (basically UO_2), exactly the same configuration reported in Fig. 3c. The same argument can be applied to the boundary layer and the SiO_2-enriched layer reported in Gusarov et al. (2006). By this comparison, it can be concluded that the present configuration is mostly due to the interaction between UO_2 and SiO_2.

It is known that silica interacting with CaO (Hillert et al., 1990), UO_2 (Ball et al., 1993) and ZrO_2 (Ball et al., 1993) may form a miscibility gap at the liquid state. Thus, this configuration represents two rapidly solidified immiscible liquids, and it is strongly influenced by silica role. The numerous phases observed within the white and black structures in Fig. 3 are the results of these interactions. The "glass former" action of SiO_2 leads to the presence of a tetrahedral network in the liquid phase. This 3D structure affects the viscosity of silica-containing liquids, which is generally greater than 10 mPa s (Ramacciotti et al., 2004). The other ions, namely Ca^{2+}, Zr^{4+} and U^{4+} are "modifiers", that is they contribute to the destruction of the tetrahedral network and thus to decreasing the viscosity of the silica-containing melt. Al^{3+} is amphoteric, and in presence of silica-based tetrahedral structures, it can replace silicon at the centre of the tetrahedral network (Benoit et al., 2001).

Gusarov et al. (2006) claimed that, due to viscosity related phenomena, the equilibrium concentrations could be attained only at high temperature (T = 2673 K). However, their experiments last only 1 min. It can be concluded that the duration of the experiments has also contributed to non-equilibrium conditions, and the elevated viscosity of the melt may have counteracted the gravitational-driven stratification process. In other words, the difference in density between the UO_2-rich and the SiO_2-rich liquids was not sufficient to lead to a stratified configuration at temperature lower that 2673 K and within the annealing time (1 min). This is confirmed by the fact that, during the present study, a stratified configuration as the one obtained in Gusarov et al. (2006) has been achieved at 2500 K with an annealing duration of 30 min.

The origin of the small droplets dispersed within Zone 1 and Zone 2 and those observed by Gusarov et al. (2006) is difficult to explain. These droplets may have been present at the annealing temperature, and then they quenched in the observed configuration. The small dimension of these droplets (maximum diameter of 2–3 μm) may alternatively suggest that they originated during the separate cooling of the immiscible liquids. When one of the two immiscible liquids enters the miscibility gap crossing a tie-line, it may reject a secondary liquid under the form of small droplets. However, the number of the rejected droplets should be limited, since the molar fraction of the secondary liquid is significantly smaller than the primary liquid, applying the lever rule to the considered tie-line. In the present case, the amount of droplets (both in Zone 1 and Zone 2) seems to be too large for accepting the second hypothesis. In Gusarov et al. (2006) no explicit interpretation is given on the formation of the droplets.

Further investigation should be performed in the future to shed light on this non-fully clarified and interesting aspect.

4. The ATTILHA setup

The ATTILHA (Advanced Temperature and Thermodynamic Investigation by Laser Heating Approach) facility was recently developed at the LM2T, CEA Saclay. Thanks to this novel high temperature experimental setup using laser heating and aerodynamic levitation, extreme temperature may be reached, allowing the measurement of the melting temperature of rather refractory materials. Furthermore, the quasi-contactless conditions during the experiments will limit the interaction between the sample and the environment. In a second more advanced version of the facility, samples containing radioactive (mostly α-emitters) materials (i.e., U and UO_2) may also be investigated.

A schematic representation of the ATTILHA setup is shown in Fig. 4.

A 250 W Coherent® CO_2 laser (λ = 10.6 μm) heats a spherical sample levitating in a controlled gas flow. In principle, any gas can be used as levitation gas. The sample is completely melted during the experiment: the homogeneity of the sample is achieved and temperature gradients limited. An infrared HgCdTe detector (1–14 μm) and a two-channel pyrometer (λ_1 = 0.8 μm, λ_1 = 1.05 μm) allow a precise temperature measurement. Spatial

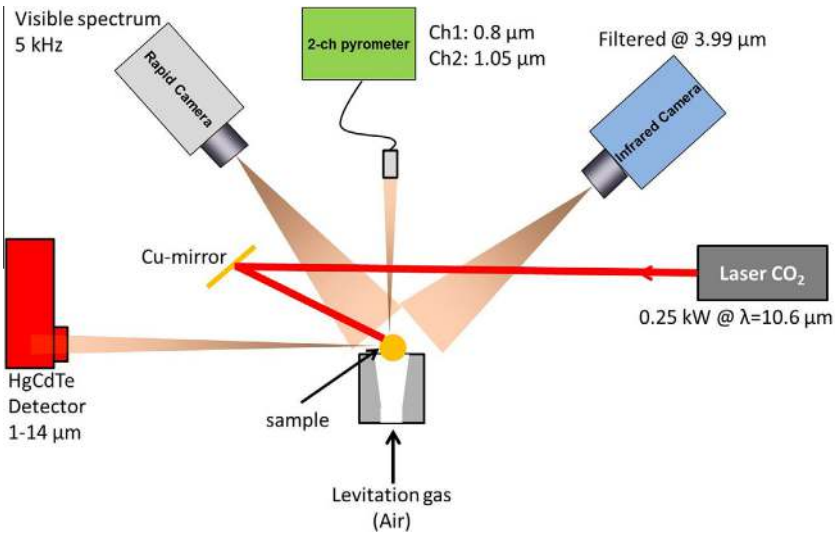

Fig. 4. Schematic representation of the ATTILHA setup.

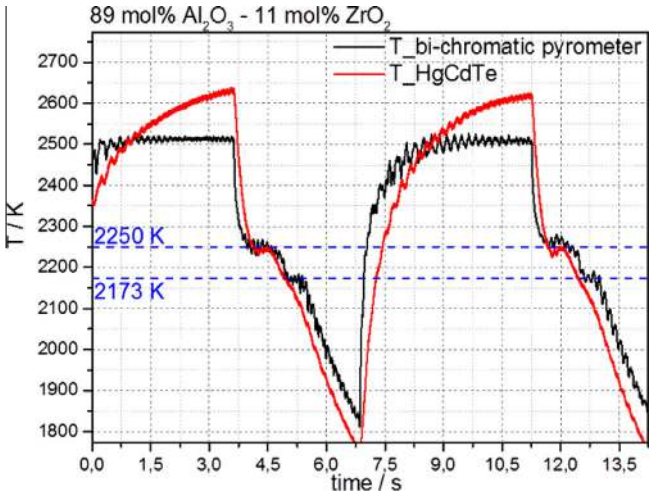

Fig. 5. Thermograms recorded with the bi-chromatic pyrometer (black line) and the HgCdTe detector (red line). It must be pointed out that, during this test, an interferential filter at 10 μm was placed between the HgCdTe detector and the sample. (For interpretation of the references to colour in this figure legend, the reader is referred to the web version of this article.)

information, such as temperature gradients or the presence of two or more phases may be observed by means of (i) a filtered infrared fast camera (3.99 μm) and (ii) a fast visible camera. Thanks to the rapid visible camera it will be possible to detect rather fast events, such as the quenching of the sample or the formation of the first drop of liquid during the heating. The synchronisation of these instruments will allow a thorough comprehension of the fusion and solidification phenomena of the investigated samples. Furthermore, if a miscibility gap exists in the liquid phase, the movements of the two immiscible liquids will be detected giving new information on their densities and on their interfacial tensions.

Preliminary results on a mixture Al_2O_3–ZrO_2 were obtained. A sample with a composition $(Al_2O_3)_{0.89}(ZrO_2)_{0.11}$ was fabricated by directly placing starting materials (Al_2O_3 99.999% purity and ZrO_2 99.9% purity) at the bottom of the nozzle. The laser was then focused onto the pure oxides. The obtained droplet-shaped sample levitated in an air stream. Thanks to the two-channel pyrometer and the HgCdTe detector, both liquidus ($T = 2250 \pm 96$ K) and eutectic ($T = 2173 \pm 70$ K) transitions temperatures are detected. These results are in good agreement with previous data (Ball et al., 1993; Harmelin, 1993). However, some uncertainties still remain on the eutectic transition temperature, with authors reporting values ranging between 1980 K (Cevales, 1968) and 2200 K (Wartenberg and Reusch, 1928). Further investigation will help resolving this inconsistency. The thermograms recorded by the pyrometer and the HgCdTe detector are reported in Fig. 5.

The temperature measured by the HgCdTe detector (in the present case a 10 μm interferential filter was placed between the HgCdTe detector and the sample) and the pyrometer differ significantly on the heating flank. While the pyrometer recorded a constant temperature, the HgCdTe recorded a rising temperature until the laser was switched off. In the working range of the pyrometer (0.8 and 1.05 μm), the transmittance of the sample cannot be considered negligible, due to its semi-transparent nature. Therefore, the pyrometer measures the radiant flux also coming from a colder zone underneath the surface of the sample, which is not directly heated by the CO_2 laser. In conclusion, the differences in the recorded thermograms are due to the variation of the optical properties of the sample as a function of the wavelength.

Fig. 6a shows a BSE image of the microstructure of the solidified sample. EDS analysis on black phase revealed that it is pure Al_2O_3, confirming that alumina does not dissolve ZrO_2. The measured eutectic composition is 31 mol% ZrO_2, which is in good agreement with results found in Ball et al. (1993) and Harmelin (1993). Thermal images from the infrared camera (Fig. 6b and c) allow study the spatial solidification behaviour of the sample. The liquid sample is semi-transparent at the wavelength of infrared camera ($\lambda = 3.99$ μm).

Fig. 6b reports an infrared frame showing the investigated sample at the liquid state. In Fig. 6c it is also possible to observe the coexistence of a liquid phase and the solid crust forming during the cooling stage of the experiment. It can be noted that the colour of the solid and liquid phases are different (the solid phase is blue whilst the liquid phase is green). Since the temperature gradients inside the sample are limited, the difference in the colour, which

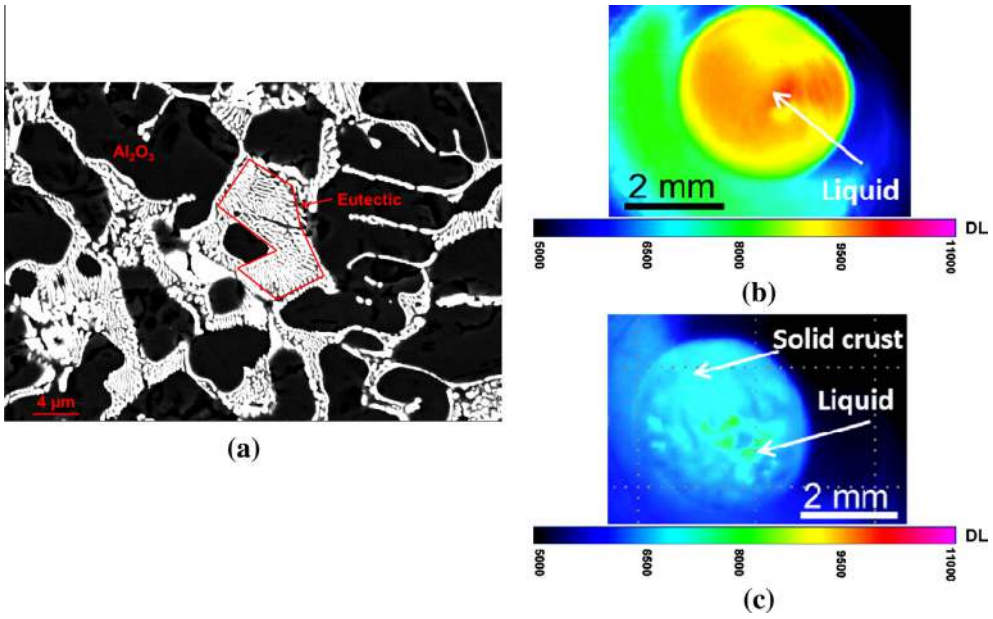

Fig. 6. Laser heating results on a $(Al_2O_3)_{0.89}(ZrO_2)_{0.11}$ sample. (a) BSE-SEM image of the microstructure of the solidified sample; (b) thermal image obtained with the filterer infrared camera on liquid sample; (c) thermal image of the sample during cooling. DL = Digital Level, which is the 14 bits output digital value from the infrared camera.

corresponds to a difference in the measured thermal flux, is mainly due to a difference in the emittance of the phases. In particular, it can be concluded that the emittance of the liquid phase is larger than that of the solid phase.

5. Conclusions and perspectives

The current annealing tests represent a first attempt of small-scale experiments investigating corium/concrete interaction. This experiment provides useful data for the comprehension of the phenomena occurring during a severe accident, when the molten corium reaches the concrete in the cavity underneath the damaged steel vessel. The advantage of small-scale annealing tests is that temperature and composition gradients are limited. While large-scale experiments give important information on the accident phenomenology, the coupling of large-scale experiments and the present approach may represent a solution for a thorough analysis of different accident scenarios.

Thanks to the present work, it can be affirmed that, depending on the SiO_2-content in the prototypic concrete interacting with the corium, the final configuration of the ex-vessel corium can be significantly different:

- The interaction with a CaO-rich concrete resulted in an homogenous dendritic microstructure, that is in a single liquid formation.
- The interaction with a SiO_2-rich concrete resulted in the formation of two immiscible liquids.

In the latter case, the presence of a miscibility gap between two liquids – one enriched in U, the other with traces of U – could be an issue from the re-criticality point of view. In fact, the accumulation of most of the available U stored in one particular region of the ex-vessel corium could cause, in the presence of moderator, a re-start of a self-sustaining fission chain.

Future investigations of this kind of mixture will allow to identify the main cause of the microstructure of solidified CORIUM_2 sample. A kinetic study on the same composition would help to understand if gravitational stratification of silica-containing melts is significantly affected by viscosity.

The ATTILHA experimental setup was recently conceived and developed. The main advantage of this facility is the possibility to perform fast measurements under aerodynamic levitation, limiting external contamination of the sample and thermal gradients. The setup was tested on the Al_2O_3–ZrO_2 system, showing its potentiality and versatility. Future improvements will allow the investigation of α-emitters-containing system.

Acknowledgments

The authors would like to thank Anne Boulin (Laboratoire de Physique et de Modélisation des Accidents graves, CEA Cadarache) for the TOLBIAC-ICB calculations.

References

Baichi, M., Chatillon, C., Guéneau, C., 2001. Mass spectrometer study of the UO_2–ZrO_2 pseudo-binary system. J. Nucl. Mater. 294, 84–87.

Ball, R.G.J., Mignanelli, M.A., Barry, T.I., Gisby, J.A., 1993. The calculation of phase equilibria of oxide core-concrete systems. J. Nucl. Mater. 201, 238–249.

Benoit, M., Ipsas, S., Tuckerman, M.E., 2001. Structural properties of molten silicates from ab initio molecular-dynamics simulations: comparison between CaO–Al_2O_3–SiO_2 and SiO_2. Phys. Rev. B 64, 224205.

Cevales, G., 1968. Phase-equilibrium diagram of Al_2O_3–ZrO_2 and examinations of a new high temperature phase (ε-Al_2O_3). Ber. Deut. Keram. Ges. 45, 216–219 (in German).

Chevalier, P.Y., Fischer, E., Cheynet, B., 2004. Progress in the thermodynamic modelling of the O–U–Zr ternary system. Calphad 28 (1), 15–40.

Guéneau, C., Dauvois, V., Pérodeaud, P., Gonella, C., Dugne, O., 1998. Liquid immiscibility in a (O, U, Zr) model corium. J. Nucl. Mater. 254, 158–174.

Gusarov, V.V., Mezentseva, L.P., Popova, V.F., Almyashev, V.I., Lomanova, N.A., Kuchayena, S.K., Khabensky, V.B., Bechta, S.V., Granovsky, V.S., Vitol, S.A., Krushinov, E.V., Kotova, S.Yu., Blisnyk, V.G., Kalyago, E.K., Lysenko, A.V., Bulygin, V.R., Shevchenko, E.V., Kamensky, N.E., Kosarevsky, R.A., Martynov, V.V., Belyaeva, E.M., Sulatsky, A.A., Shuvalov, S.V., 2006. Investigation of binary oxidic systems: UO2–SiO2 system, CORPHAD Phase 2, Progress Report 01/05/06-30/11/06, ISTC Project-1950.2 CORPHAD.

Harmelin, M., 1993. Aluminium–Oxygen–Zirconium. Ternary Alloy, vol. 8. VCH, pp. 89–93.

Hillert, M., Sundman, B., Wang, X., 1990. An assessment of the CaO–SiO_2. Metall. Trans. B 21B, 303–312.

Journeau, C., Piluso, P., 2012. Core Concrete Interaction. In: Comprehensive Nuclear Materials, Elsevier, pp. 635–654.

Journeau, C., Sudreau, F., Magne, S., Cognet, G., 2001. Physico-chemical analyses and solidification path reconstruction of multi-component oxidic spread melts. Mater. Sci. Eng. A 299, 249–266.

Juenke, E.F., White, J.F., 1970. Physico-chemical Studies of Clad UO2 Under Reactor Accident Conditions, General Electric Company, Report GEMP-731.

Quaini, A., Guéneau, C., Gossé, S., Bracks, E., Hodaj, F., submitted for publication. J. Nucl. Mater.

Ramacciotti, M., Journau, C., Sudreau, F., Cognet, G., 2004. Viscosity model for corium melts. Nucl. Eng. Des. 204, 377–389.

Spindler, B., Tourniaire, B., Seiler, J.M., 2006. Simulation of MCCI with TOLBIAC-ICB code based on the phase segregation model. Nucl. Eng. Des. 236, 2264–2270.

TAF-ID, 2015. <www.oecd-nea.org/science/taf-id>.

Wartenberg, H., Reusch, H.J., 1928. The melting diagram of some high-refractory oxide. IV (Aluminium oxide). Z. Anorg. Allg. Chem. 207, 1–20 (in German).